Electrical property modulation of Au/Ba0.6Sr0.4TiO3/La0.7Sr0.3MnO3 structure by continuous composition spread Mn doping

Jie Qiu, Guozhen Liu, Jerome Wolfman, Jie Xing

Electrical property modulation of $Au/Ba_{0.6}Sr_{0.4}TiO_3/La_{0.7}Sr_{0.3}MnO_3$ structure by continuous composition spread Mn doping

Jie Qiu[a], Guozhen liu[a*], Jerome Wolfman[b**], and Jie Xing[c]

[a] Jiangsu Key Laboratory of Micro and Nano Heat Fluid Flow Technology and Energy Application, School of Physical Science and Technology, Suzhou University of Science and Technology, Suzhou, 215009, China

[b] Laboratoire GREMAN, UMR 7347 CNRS, Université François Rabelais, Parc de Grandmont 37200 Tours, France

[c] School of Science, China University of Geosciences, Beijing 100083, China

Abstract

Composition spread Mn-doped $Ba_{0.6}Sr_{0.4}Ti_{1-x}Mn_xO_3$ (BSTM*x*, $0 \le x \le 0.05$) thin films have been prepared on $La_{0.7}Sr_{0.3}MnO_3/SrTiO_3$ (LSMO/STO) layer by combinatorial pulsed laser deposition. When *x* is less than 1.67 %, the BSTM*x* films are single phase according to X-ray diffraction patterns, and the Au/BSTM*x*/LSMO structure present asymmetry transport properties. The reverse-bias current of Au/BSTM*x*/LSMO structure remains at low value of 10^{-10} A. The forward-bias current, however, reduces rapidly with the ascending doping content. The asymmetry transport property gets weak with Mn doping concentration. The positive and negative currents increase rapidly, and are close as Mn content is greater than 3.75 mol% indicating the disappearance of the asymmetric transport property. The effects of the LSMO electrode, Au/BSTM*x* Schottky junction, BSTM*x* thin film, and BSTM*x*/LSMO interface on the whole electrical transport properties are discussed by virtue of the experimental and fitting impedance spectrums. Our results are helpful for the insight into the doping physical mechanisms in perovskite oxides.

Key words: ferroelectric thin films; heterostructures; transport properties; dielectric properties; pulsed laser deposition

*Corresponding author. *E-mail address*: guozhen.liu@hotmail.com.

**wolfman@univ-tours.fr

1. Introduction

The characteristics of oxide heterostructures can be controlled by combining two or more materials with similar or distinct properties together, and have attracted increasing attention due to their potential application in memories, sensors and other microelectronics [1-4]. As artificial structures, oxide heterostructures as well as supperlattices and multilayers offer a chance to explore novel materials, such as new superconductor and multiferroic materials [5]. Oxide multiferroic heterostructures integrating ferroelectric and ferromagnetic materials show unique multifunctionality and superior performances, hence are good candidates for energy harvesters, magnetic sensors, tunable resonators and phase shifters [6-7]. As an excellent ferromagnetic material with Curie temperature just above room temperature, $La_{0.7}Sr_{0.3}MnO_3$ (LSMO) is one of ideal materials for constructing these multiferroic heterostructures. In addition, the perovskite structure of LSMO compound makes a good lattice match to most of other ferroelectrics like $Ba_{0.6}Sr_{0.4}TiO_3$ (BST) [8, 9]. Among the lead free ferroelectrics, BST is well known for its high dielectric constant, high dielectric tunability at room temperature [10]. However, BST thin films also undergo large leakage current due to the electron hopping between Ti^{4+} and Ti^{3+} [11]. It has been noted that Mn-doped titanates showed largely reduced leakage current since the acceptor-type dopants, such as Mn^{2+} and Mn^{3+}, could compensate the donor charges from the reduction of Ti^{4+} to Ti^{3+} and correspondingly suppress the electron hopping between titanate ions [12]. So far, there are a few investigations about Mn-doped BST compounds, in which the Mn doping mole content varied from 0 % to 5 % [13-15]. However, the optimal doping concentration in single phase BST single crystals is still not clear, and thus a systematic study with continuous Mn composition spread in BST thin films is necessary. In current study, we prepare composition spread $Ba_{0.6}Sr_{0.4}Ti_{1-x}Mn_xO_3$ (BSTM*x*, $0 \leq x \leq 0.05$) thin films by combinatorial pulsed laser deposition (Comb-PLD), and present a detailed analysis of the structure, dielectric and electrical transport properties of Au/BSTM*x*/LSMO structure. Our results show that the BSTM*x* thin films maintain single phase when *x* is less than 1.67 %, and then present a second phase if Mn content increase further. The forward-bias current at a bias of 6 volts rapidly reduce with ascending Mn content *x* ($x < 1.7$ %), and reduce by four orders of magnitude when $x = 1.5$ %. However, the reverse-bias current is

almost insensitive of the doping concentration, and remain at the order of 10^{-10} A. The trap-filling limit current and the enhanced barrier height of the Au/BSTM*x* Schottky junctions are used to explain the transport properties. Our results suggest a feasible way to obtain Schottky or p-n junctions with tunable onset voltages, and indicate the Mn optimized concentration in single phase BST or others perovskite oxide thin films.

2. Experimental procedure

The BSTM*x*/LSMO structures were fabricated on (001) $SrTiO_3$ (STO) substrates by laser ablation. Firstly an epitaxial LSMO layer with a thickness of 100 nm was grown on a 10 mm by 10 mm STO single crystal substrate by focusing a KrF excimer laser on a stoichiometric LSMO target. The dynamic oxygen pressure was 0.3 mbar and the substrate temperature was 700 ^oC during the growth. Maintaining the substrate temperature, the LSMO film was then *in situ* annealed in 0.5 bar oxygen for 45 minutes to minimize the oxygen vacancies and improve the crystal quality of the LSMO film. For the 300-nm-thick BSTM*x* thin films, the deposition was assisted by a synchronized shutter motion and laser firing control system, named as Comb-PLD. In current Comb-PLD method, the desired composition spread along horizontal direction *x* and remained constant in vertical direction *y*. Details of the Comb-PLD procedure were described in our previous papers [16-18]. The targets used for the BSTM-*x* films in the Comb-PLD were BST and $Ba_{0.6}Sr_{0.4}Ti_{0.95}Mn_{0.05}O_3$ ceramics. The oxygen pressure and substrate temperature for the growth of BSTM-*x* thin film were 0.1 mbar and 600 ^oC, respectively. After the deposition, the BSTM*x*/LSMO structures were cooled down to room temperature in 0.8 bar oxygen with a rate of 10 ℃/min. The crystal structure of the BSTM*x*/LSMO structures was checked by high resolution x-ray diffractometer (HRXRD). A 50-μm-wide slit was used during the HRXRD measurement, which resulting in a 100-μm-wide beam footprint in the *x* direction. Top Au contacts with an area of 0.05 mm^2 were sputtered at room temperature through a shadow mask for electrical measurements. The dielectric properties were measured by a HP4294A impedance analyzer with a 30 mV oscillation voltage. The current-voltage characteristics of the Au/BSTM*x*/LSMO structure were measured by a Keithley 236 source-measure unit.

3. Results and discussion

3.1. Structural analysis

Figure 1 shows the XRD theta-2theta patterns around STO (002) peak of pure and Mn-doped BST films. The step for each local composition measurement is 1.0 mm along *x* direction. Only (002) peaks of the LSMO layer was observed, indicating a highly oriented single phase LSMO layer was obtained. It was also noted the finite thickness fringes appearing around the LSMO (002) main peak, suggesting that a smooth surface of the LSMO layer was achieved [19]. The BSTM*x* (002) peak shifts from 45.28 degree for $x = 0$ to 46 degree for $x = 0.33\%$, and vanishes when $x \geq 3.89$ %. Meanwhile, two sets of unknown "impure" peaks marked by solid dots and diamonds appear when $x \geq 2.22$ %, and gets stronger with Mn content. The evolution of the XRD patterns of BSTM*x*/LSMO structures on STO substrates suggests a structural reconstruction in BSTM*x* thin films. Compared with the literature in which BSTM*x* ceramics maintained in single phase when $x \leq 6$ % [15], the BST films here had smaller incorporation limit of around 1.67 %, which could be ascribed to the perfect single crystal structure, the interfacial strain effect and Mn cation intermixing at the LSMO/BSTM interface at high temperature [20].

3.2. Electrical properties

Figure 2 shows the capacitance map of the Au/BSTM*x*/LSMO capacitors at 10 kHz. The map was composed of 160 capacitors distributing at 8 rows and 20 columns. In other words, 20 local compositions were checked, and 8 capacitors were measured for each composition. It can be seen the dielectric constants are almost uniform in *y* direction, and change monotonously in *x* direction. Considering that the dielectric constant of $Ba_{1-x}Sr_xTiO_3$ compounds is highly related with the composition, the dielectric constant map shown in Fig. 2 actually reflected the composition distribution of BSTM*x* thin films. The dielectric constant of BSTM*x* thin films reduced with the increasing Mn concentration, which is in consistent with other results in single Mn-doped BST films grown by PLD or sol-gel method [13, 15]. The Fig. 3 shows that the capacitance (permittivity) of the Au/BSTM*x*/LSMO structures reduces with the applied which is compliance with the dielectric tunability theory. The symmetric bias-dependent capacitance will give us useful information in later discussion.

The transport properties of the Au/BSTM*x*/LSMO structure were measured as forward biases were applied to the top Au electrode. The leakage current (on a log scale) versus voltage (*I*-*V*) characteristics of the Au/BSTM*x*/LSMO structure for $x = 0$, 0.5, 1.0

and 1.5 % are shown in Fig. 4 (a). The *I-V* curves exhibited an apparently asymmetric characteristic. The forward-bias currents were much greater than the reverse-bias currents, especially for x = 0 which shows five orders of magnitude difference between the two currents when 6 V was applied.

Figure 4(b) shows the dependence of currents on Mn doping concentration when 6 V bias was applied. It can be seen that the forward-bias current reduced rapidly with increasing Mn content first when x < 3.75 mol %, and then remained at a low value of around 10^{-9} A when 1.75 < x < 3.75 mol %, whereafter increase rapidly with Mn doping content. On the other hand, the reverse-bias current almost remained at around 10^{-10} A when 0 ≤ x ≤ 1.75 mol %, subsequently rise with Mn concentration. So the shallow Mn doping concentration is an effective way to reduce the leakage current of BST thin films. When the Mn content is greater than 3.75 mol%, the positive and negative current are almost close which indicates the presence of the symmetric *I-V* curves.

The asymmetric transport characteristics shown in Fig.4 (a) could be related to the asymmetric bottom and top interfaces. The work function is about 5.2 eV for Au, and about 4.8 eV for LSMO thin films [21-23]. The electron affinity of BST thin films and band gap are about 4.0 eV and 3.2 eV, respectively [24]. So, a Schottky barrier could be built at the Au/BSTM*x* rather than LSMO/BSTM*x* interface, regarding to an *n*-type conductive mechanism in BSTM*x* layer. The speculation built on the basis of metal work function and BSTM*x* electron affinity is consistent with the asymmetric transport properties of the Au/BSTM*x*/LSMO structure. When a forward bias was applied to the Au electrode, the barrier height for the forward biased Au/BSTM*x* Schottky junction was lowered，and then the carrier electrons were injected into Au/BSTM*x*/LSMO structure. For a Schottky junction, a linear relationship between ln(J) and the electric field E was described by Eq. 1. [25, 26]

$$\ln J = \frac{eV}{k_B T} + \ln A^* T^2 - \frac{e\phi_{Bn}}{k_B T} \quad (1)$$

Where e is the electron charge, k_B Boltzmann′s constant, T the temperature, A^* the Richardson constant, ϕ_{Bn} the effective Schottky barrier height.

The slope S_s of ln(J)-V curve for a Schottky junction is specified by Eq. 2 as follows:

$$S_s = \frac{e}{k_B T} \quad (2)$$

Indeed, a linear ln(J)-V curve of Au/BSTMx Schottky junction under forward biases was shown in Fig. 4 (a). The slope varied from 2.2 to 1.2, which is deviated from to the room-temperature value of 40 indicating that there is another mechanism involving in the transport properties.

Some other basic conduction processes such as Ohmic law and space charge limited current are known in oxides. The relationships between the current densities J and the applied biases V are presented as follows:[27]

For Ohmic law, the current density J may be written as

$J = q\mu nV/L$ (3)

For trap-free insulators, the space charge limited current (SCLC) density J, is expressed by Eq. 4

$J = \varepsilon\varepsilon_0\mu V^2/L^3$ (4)

For insulators with traps distributed in energy, the trap-filling limit current (TFLC) is a high power function of voltage can be represented by Eq. 5

$I \propto V^{(T_C/T)+1}$ (5)

Where μ and n are the carrier mobility and density, respectively; L is the space span between electrodes. T_c is a characteristic temperature greater than the temperature at which I - V curves are measured. So the linear relationships between ln$J$ and ln$V$ will setup for all three conduction mechanisms specified by eqs. (3), (4) and (5), and the slopes of ln$J$ – ln$V$ curves are 1 for Ohmic law, 2 for SCLC and greater than 2 for TFLC, respectively.

The ln$J$ – ln$V$ curves of Au/BSTMx/LSMO structure under greater than the onset voltages were shown in Fig. 5. Above the onset voltages, the slopes for all structures with various Mn contents were greater than 2 varying from 9.5 for x=0.0 mol% to 5.6 for x=1.5 mol%, which indicated that these structures shared the same TFLC conductive mechanism. A decrease in the slopes of ln$J$ – ln$V$ curves with increasing Mn content suggests that the trap concentration in BSTMx thin films decline with the ascending Mn doping concentration. The lower trap concentration in BSTMx thin films gives rise to the greater thin films resistance value as can be confirmed by the impedance analysis.

The impedance spectrums from 1000 Hz to 6.3 MHz are shown in Fig.6 (a). The good agreements between the experimental scattered curves and the corresponding fitting solid lines indicate that the equivalent circuits (shown in Fig. 6(b)) of samples have been successfully set up. The fitting parameters are listed in Tab. 1. The R_1 is related with the resistance of the LSMO bottom electrodes which varies from 200 to 345 Ω due to the variation of sample positions. As can be seen from Tab.1, the magnitude of R_2 is several orders of magnitude greater than other resistances, so the voltages are applied mainly to the R_2 and C_2 elements in parallel. Considering the symmetric *C-V* diagrams of all samples, the C_2 and R_2 elements come from the BSTM*x* thin film. The capacitance C_2 reduces with the ascending manganese concentration as shown in Tab.1 which is consistent with the position dependent capacitance as shown in Fig. 2. Meanwhile the resistance R_2 increases with the Mn content as suggested by *I-V* curves.

The complex impedance spectrum at high frequencies (above 1.0 MHz) is sensitive to the magnitude of the R_3 and *CPE3* elements in parallel which are correlated with the ohmic contact at BSTM*x*/LSMO interface. The Mn element as an acceptor impurity give rise to the carrier hole concentration in BSTM*x* thin films, and make the Fermi level move to the top of the valence-band energy. It will result in a more desirable ohmic contact at BSTM*x*/LSMO interface. According to the impedance fitting data, the magnitude of resistance R_3 reduces with Mn doping concentration from 1600 Ω for x=0.0 mol% to 380 Ω for x=1.5 mol%. The *CPE* element is a perfect capacitor when the *CPE-P* value is equal to 1. While the *CPE-P* value drops to 0, the *CPE* element declines to a resistor. The *CPE-P3* magnitude varies from 0.394 to 0.798 with Mn content shown in Tab. 1 indicates the coexistence of resistance and capacitance characteristics at BSTM*x*/LSMO interface.

So the last R_4 and *CPE4* elements in parallel in Tab. 1 are correlated with the Au/BSTM*x* Schottky junction. The increase in R_4 magnitude with the Mn doping concentration indicates an increment in the effective barrier height of the Au/BSTM*x* Schottky junction. The *CPE-T4* magnitude reduces from 11.05 nF to 6.53 nF indicating an increase in the width of depletion region of Au/BSTM*x* Schottky junction and a decrease in the carrier electron concentration according to Eq. 6 and 7, respectively [25, 26].

$$C = \varepsilon_0 \varepsilon_r \frac{A}{W} \quad (6)$$

$$W = \sqrt{\frac{2\varepsilon_0 \varepsilon_r V_{bi}}{eN}} \quad (7)$$

According to the fitting results, the capacitance of the Au/BSTM*x* Schottky junction is about 12 times than that of BSTM$_x$ thin films. On the other hand, the resistance of BSTM$_x$ thin films is about 18 times than that of the Schottky junction. This means that only about one eighteenth voltages were applied to the Schottky junctions. If the forward applied voltage magnitude is divided by 18 first, then the slopes of ln(*J*)-*V* curve for the Au/BSTM*x* Schottky junction is around 40 in compliance with Eq. 2 at room temperature. In other words, the transport properties of the Au/BSTM*x* Schottky junction under forward-bias voltage were triggered by the TFLC mechanisms in the BSTM*x* thin films, meanwhile were controlled by the Au/BSTM*x* interface.

As also shown in Fig. 3a, the forward leakage current reduced with the increasing Mn content. Moreover, the forward onset voltages where the current rapidly increased were 1.2, 1.5, 1.9 and 2.1 V, respectively, for x = 0, 0.5, 1.0, 1.5 mol %. The rising thin film resistance R_2 suggests that BSTM$_x$ thin film will share more positive bias voltage. It means that a greater bias is needed to open the Au/BSTM*x* Schottky junction. It was reported that the addition of Mn into a nominally undoped $Ba_{0.5}Sr_{0.5}TiO_3$ thin film produced a remarkable increase in the barrier height of Pt/$Ba_{0.5}Sr_{0.5}TiO_3$ Schottky junction [12]. Similarly, the barrier height of the Au/BSTM*x* junction would increase just like the resistance R_4 rising with Mn content shown in Tab. 1.

When a reverse-bias voltage was applied to the Au electrodes, the barrier height for the reverse biased Au/BSTM*x* junction was ascended. The reverse-biased leakage current was kept at a low level of 10^{-10} A, which is almost insensitive to the Mn content. So the electrical conductive carriers were produced by the TFLC mechanism, and then controlled by a Schottky junction.

A number of oxygen vacancies were produced during the growth of the BST thin film which can be expressed as follows [28,29]

$$O_O \leftrightarrow V_{\ddot{O}} + \frac{1}{2}O_2 + 2e^{'} \quad (6)$$

where O_O is an electrically neutral oxygen atom, $V_O^{\cdot\cdot}$ represents a positive charged oxygen vacancy, $e^{'}$ denotes a negative charged electron. The oxygen vacancies would act as trapping centers for free electrons. Meanwhile, some Ti^{4+} ions would change to Ti^{3+} ions to keep electrical neutral BST thin films for the presence of oxygen vacancies. The hopping of the free electrons between Ti^{3+} and Ti^{4+} ions would lead to the electrical conduction of BST thin film. The partial substitution of Mn^{3+} ions for Ti^{4+} ions would suppress the forming of oxygen vacancies and the hopping probability of electrons between Ti^{4+} and Ti^{3+} ions [30]. Correspondingly, the leakage current would reduce with the ascending Mn doping concentration as shown in Fig. 4 (b). In other words, Mn element acts as an acceptor impurity in BSTM*x* thin films. The minority carrier hole concentration will increase with Mn doping concentration, which give rise to the electron-hole recombination rate and reduce the leakage current of Au/BSTM*x*/LSMO structure. While the Mn doping concentration rises up to 3.75 mol%, it would lead to a surplus in the carrier holes and make the current go up.

In conclusion, composition spread BSTM*x* thin films were successfully fabricated on LSMO/STO substrates by combinatorial pulsed laser deposition and the leakage current of the Au/BSTM*x*/LSMO structure was studied. X-ray diffraction results showed that the BSTM*x* thin films were single phase when $x \leq 1.67$ %. The *I*-*V* characteristics of the Au/BSTM*x*/LSMO structure showed apparent asymmetric transport properties when $x \leq 1.67$ %. The slope magnitude of the linear ln*J* versus ln*V* curves indicated that the forward current of Au/BSTM*x*/LSMO structure was triggered by the TFLC mechanism. The impedance spectrums of the Au/BSTM*x*/LSMO structure were successfully fitted by virtue of the equivalent circuit model. The fitting parameters clarified the contributions of LSMO bottom electrodes, BSTM*x* thin films, BSTM*x*/LSMO interfaces and Au/BSTM*x* Schottky junctions to the whole impedance spectrums. The fitting parameters were also used to explain the transport properties of Au/BSTM*x*/LSMO structures. The Mn doping in BST thin films resulted in a rapid decrease in forward-bias current and a slow decrease in the reverse-bias current when $x \leq 1.67$ %. Meanwhile, a slight decrease in the reverse current of Au/BSTM*x*/LSMO structure with ascending Mn content could be ascribed to the decrease in electron-hole recombination rate and carrier hopping probability. Our results suggest that the impunity doping concentration significantly affects the properties

of the oxide single crystals and oxide heterostructures, and provide useful information for the insight into the transport mechanism in perovskite oxides and the design of electronic devices like the onset voltage tunable p-n junctions or heterostructures.

Acknowledgements: This work has been supported by the National Natural Science Foundation of China (Grant Nos. 12074282, 11974318), Suzhou Key Laboratory for Low Dimensional Optoelectronic Materials and Devices (SZS201611), and Jiangsu Key Disciplines of the Thirteenth Five-Year Plan (20168765).

Figures

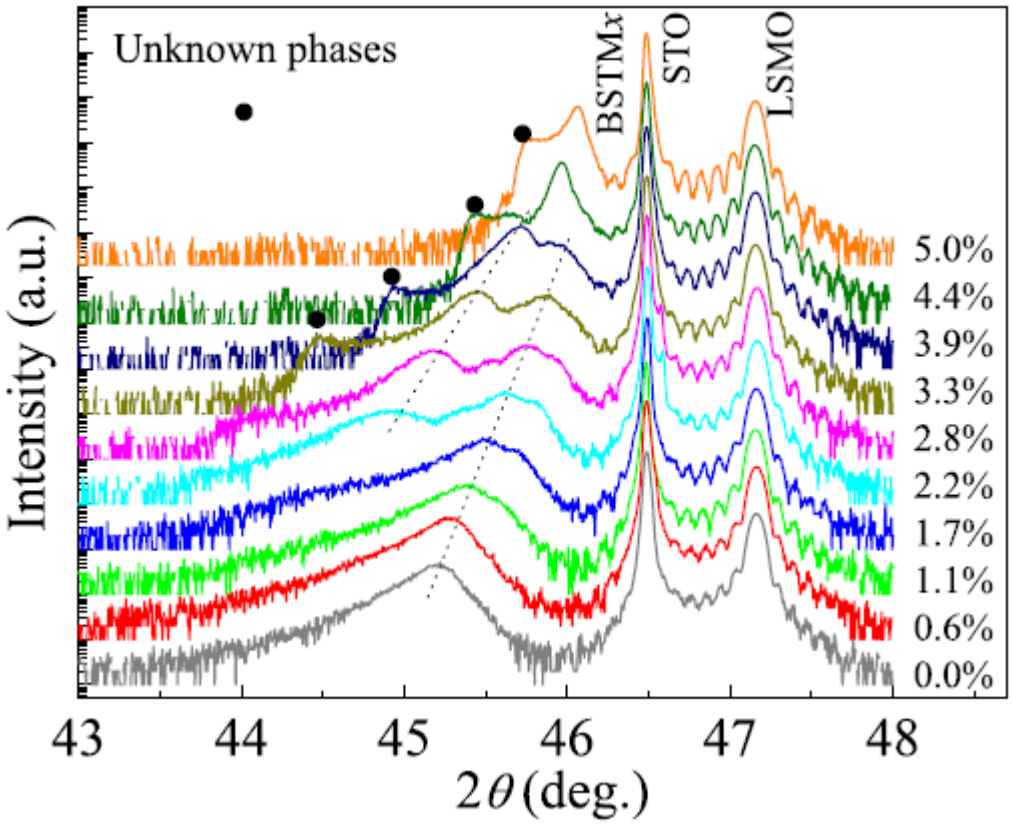

Figure 1 XRD patterns of BSTM*x*/LSMO/STO structure around (002) peak.

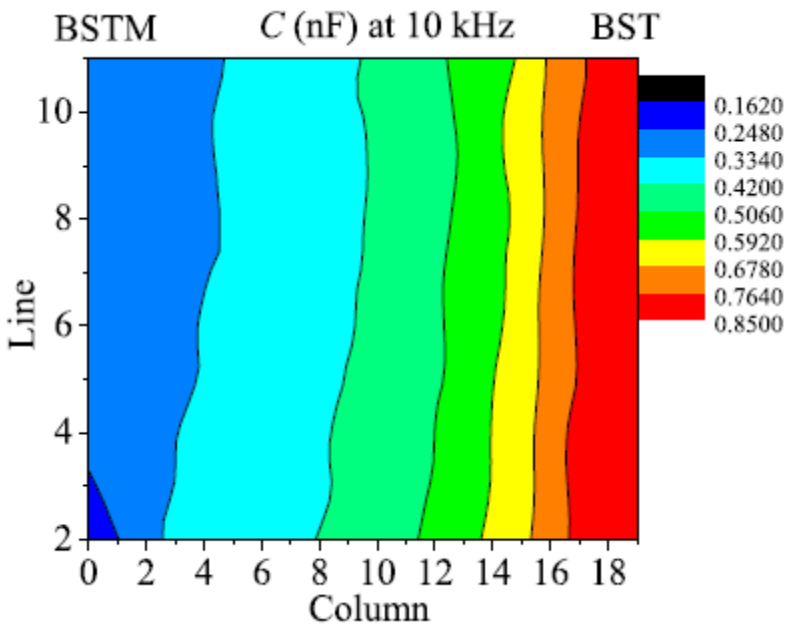

Figure 2 The contour plot of the capacitance of BSTM*x* thin films along *x* axis at 10 kHz.

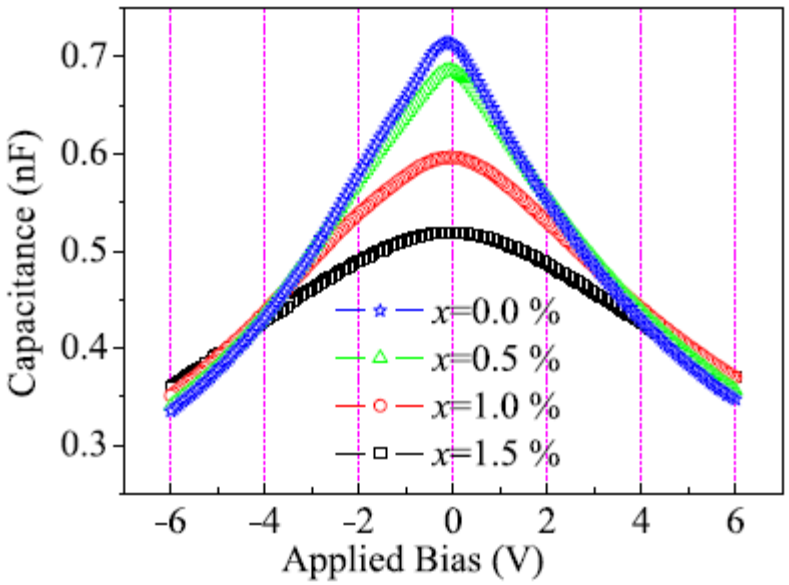

Figure 3 The capacitance-bias curves of the Au/BSTM*x*/LSMO structures.

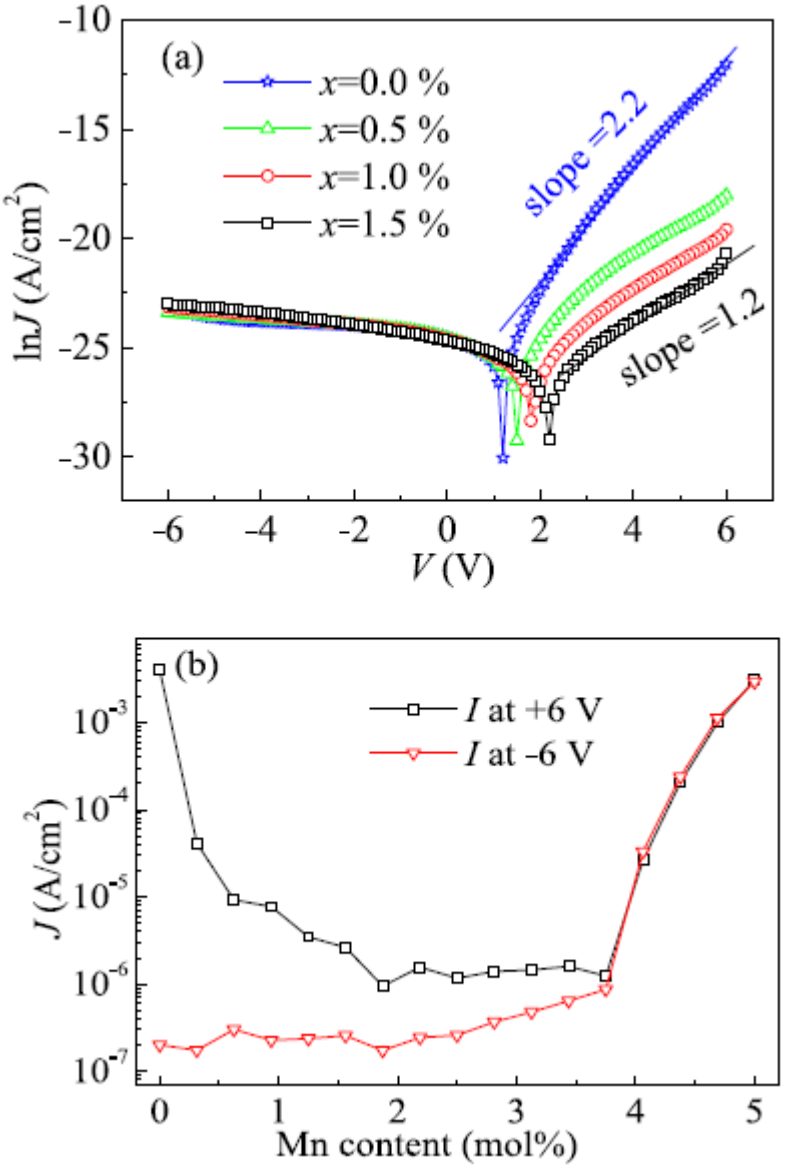

Figure 4 (a) The leakage current versus applied voltage curves of the Au/BSTM*x*/LSMO structure for x = 0, 0.5, 1.0 and 1.5 %. (b) Mn content dependent leakage current of Au/BSTM*x*/LSMO structure under forward and reverse biases.

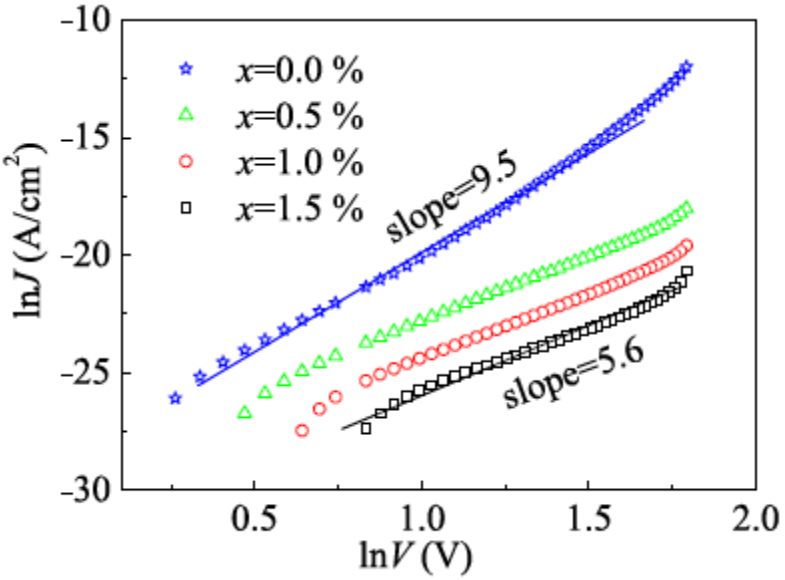

Figure 5 The ln$J$-ln V curves of Au/BSTMx/LSMO structure under forward biases.

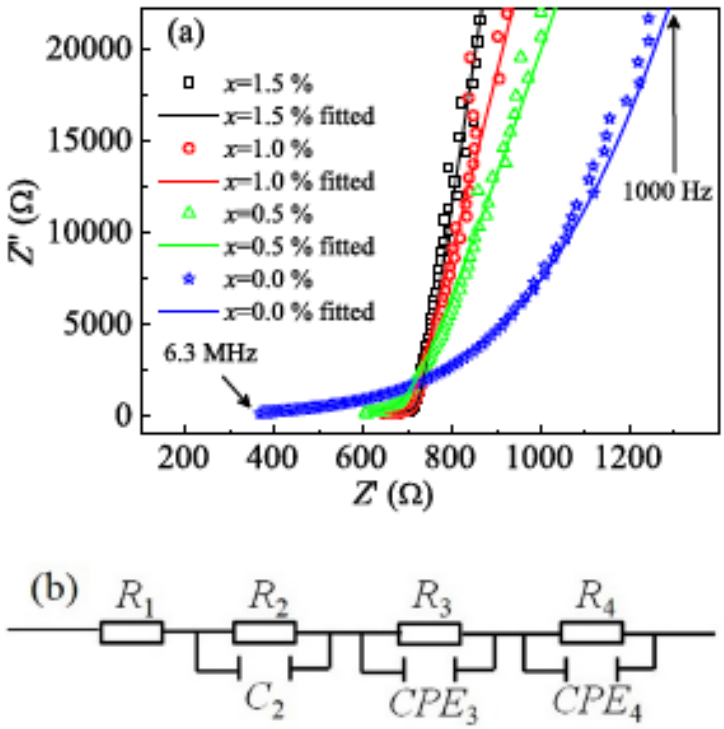

Figure 6 (a) The impedance spectrums. (b) The equivalent circuit model of Au/BSTMx/LSMO structure.

Table captions:

Table 1 The fitting parameters of the equivalent circuit of Au/BSTM*x*/LSMO structure.

References:

[1] P. Zubko, S. Gariglio, M. Gabay, P. Ghosez, and J.-M. Triscone, Interface physics in complex oxide heterostructures, Annual Review of CondensedMatter Physics, Annu. Rev. Condens. Matter. Phys 2 (2011) 141-165.

[2] S. Chen, J. L. Zhao, Q. Jin, S. Lin, S. R. Chen, H. B. Yao, J. O. Wang, Z. Fan, E. J. Guo, and H. Z. Guo, Strain-mediated insulator–metal transition in topotactically hydro-reduced $SrFeO_2$, Sci. China Phys Mech. 64 (2021) 287711.

[3] K. J. Jin, H. B. Lu, Q. L. Zhou, K. Zhao, B. L. Cheng, Z. H. Chen, Y. L. Zhou, and G. Z. Yang, Positive colossal magnetoresistance from interface effect in *p-n* junction of $La_{0.9}Sr_{0.1}MnO_3$ and $SrNb_{0.01}Ti_{0.99}O_3$, Phys. Rev. B 71 (2005) 184428.

[4] K. J. Jin, K. Zhao, H. B. Lu, L. Liao, and G. Z. Yang, Dember effect induced photovoltage in perovskite p-n heterojunctions, Appl. Phys. Lett. 91 (2007) 081906.

[5] G. Z. Liu, C. Wang, C. C. Wang, J. Qiu, M. He, J. Xing, K. J. Jin, H. B. Lu, G. Z. Yang, Effects of interfacial polarization on the dielectric properties of $BiFeO_3$ thin film capacitors, Appl. Phys. Lett. 92 (2008) 122903.

[6] N. A. Hill, Why Are There so Few Magnetic Ferroelectrics?, J. Phys. Chem. B 104 (2000) 6694-6709.

[7] N. A. Spaldin and M. Fiebig, The renaissance of magnetoelectric multiferroics, Science, 309 (2005) 391-392.

[8] L. Wang, Z. Wang, K. J. Jin, J.Q. Li, H. X. Yang, C. Wang, R. Q. Zhao, H. B. Lu, H. Z. Guo, and G. Z. Yang, Appl. Phy. Lett. 102 (2013) 242902.

[9] C. Ge, K. J. Jin, L. Gu, L.C. Peng, Y. S. Hu, H. Z. Guo, H. F. Shi, J. K. Li, J. O. Wang, X. X. Guo, C. Wang, M. He, H. B. Lu, and G. Z. Yang, Adv. Mater. Interfaces, 2 (2015) 1500407.

[10] C. Wang, B. L. Cheng, S. Y. Wang, H. B. Lu, Y. L. Zhou, Z. H. Chen, and G. Z. Yang, Improved dielectric properties and tunability of multilayered thin films of

$(Ba_{0.80}Sr_{0.20})(Ti_{1-x}Zr_x)O_3$ with compositionally graded layer, Appl. Phys. Lett. 84 (2004) 765.

[11] Z. Yuan, Y. Lin, J. Weaver, X. Chen, and C. L. Chen, G. Subramanyam, J. C. Jiang, E. I. Meletis, Large dielectric tunability and microwave properties of Mn-doped thin films, Appl. Phys. Lett. 87 (2005) 152901.

[12] S. S. Kim, C. Park, Leakage current behaviors of acceptor- and donor-doped $(Ba_{0.5}Sr_{0.5})TiO_3$ thin films, Appl. Phys. Lett.75 (1999) 2554.

[13] S. B. Lu, Z. K. Xu, Unusual strain dependence of tunability in highly (100)-oriented Mn-doped barium strontium stannate titanate thin films, Appl. Phys. Lett. 92 (2008) 232907.

[14] X. H. Zhu , D. N. Zheng, W. Peng, J. Li, Y. F. Chen, Enhanced dielectric properties of Mn doped $Ba_{0.6}Sr_{0.4}TiO_3$ thin films fabricated by pulsed laser deposition, Mater. Lett. 60 (2006) 1224-1228.

[15] X. H. Sun, P. Feng, J. Zou, M. Wu, and X. Z. Zhao, The dielectric and tunable properties of Mn doped $(Ba_{0.6}Sr_{0.4})_{0.925}K_{0.075}TiO3$ thin films fabricated by sol-gel method, J. Appl. Phys. 105 (2009) 034104.

[16] G. Z. Liu, J. Wolfman, C. Autret-Lambert, J. Sakai, S. Roger, M. Gervais, F. Gervais, Microstructural and dielectric properties of $Ba_{0.6}Sr_{0.4}Ti_{1-x}Zr_xO_3$ based combinatorial thin film capacitors library, J. Appl. Phys. 108 (2010) 114108.

[17] J. Qiu, G. Liu and J. Wolfman, Effects of electrode resistance on the dielectric behaviors of $Au/Ba_xSr_{1-x}TiO_3/La_{1.1}Sr_{0.9}NiO_4$ capacitors, Surf. Rev. Lett. 23 (2016) 1650028.

[18] J. Qiu, G. Liu, J. Wolfman, C. Autret-Lambert, S. Roger and J. Gao, Structure and dielectric characteristics of continuous composition spread $Ba_{1-x}Sr_xTiO_3$ thin films by combinatorial pulsed laser deposition, Ceram. Int. 42 (2016) 6408.

[19] H. N. Lee, S. M. Nakhmanson, M. F. Chisholm, H. M. Christen, K. M. Rabe, D. Vanderbilt, Suppressed dependence of polarization on epitaxial strain in highly polar ferroelectrics, Phys. Rev. Lett. 98 (2007) 229901 .

[20] N. Nakagawa, H. Y. Hwang and D. A. Muller, Why some interfaces cannot be sharp, nat. mater. 5 (2006) 204.

[21] M. Minohara, I. Ohkubo, H. Kumigashira, and M. Oshima, Band diagrams of spin tunneling junctions $La_{0.6}Sr_{0.3}MnO_3$/Nb: $SrTiO_3$ and $SrRuO_3$/Nb:$SrTiO_3$ determined by in situ photoemission specroscopy, Appl. Phys. Lett. 90 (2007) 132123.

[22] M. P. de Jong, V. A. Dediu, C. Taliani, W. R. Salaneck, Electronic structure of $La_{0.7}Sr_{0.3}MnO_3$ thin films for hybrid organic/inorganic spintronics applications, J. Appl. Phys. 94 (2003) 7292.

[23] D. W. Reagor, S. Y. Lee, Y. Li and Q. X. Jia, Work function of the mixed-valent manganese perovskites, J. Appl. Phys. 95 (2004) 7971.

[24] J. F. Scott, Device physics of ferroelectric thin-film memories, Jpn, J. Appl. Phys. 38 (1999) 2272-2274.

[25] Sze S. M., *Physics of Semiconductor Devices* (Wiley, New York) 1981.

[26] D. A. Neamen, *Semconductor Physics and Devices Basic Principles*, (McGraw-Hill Education (Asia) Co. and Tsinghua University press, Beijing) 2003.

[27] A. Rose, Space-charge-limited current in solid, Phys. Rev. 97 (1955) 1538.

[28] Z. T. Xu, K. J. Jin , L. Gu, Y. L. Jin, C. Ge, C. Wang, H. Z. Guo, H. B. Lu, R. Q. Zhao, and G. Z. Yang, Evidence for a crucial role played by oxygen vacancies in $LaMnO_3$ resistive switching memories, Small, 8 (2012) 1279.

[29] X. S. Wang, L. Zhou, M. X. Li, Y. Luo, T. Y. Yang, T. L. Wu, X. L. Li, K. J. Jin, E. J. Guo, L. F. Wang, X. D. Bai, W. F. Zhang, and H. Z. Guo, Surface protonation and oxygen evolution activity of epitaxial $La_{1-x}Sr_xCoO_3$ thin films, Sci. China Phys Mech. 63 (2020) 297011.

[30] C. C. Wang, G. Z. Liu, M. He, and H. B. Lu, Low-frequency negative capacitance in $La_{0.8}Sr_{0.2}MnO_3$/Nb-doped $SrTiO_3$, Appl. Phys. Lett. 92 (2008) 052905.

Table 1

ID	R_1	R_2	C_2	R_3	*CPE-T3*	*CPE-P3*	R_4	*CPE-T4*	*CPE-P4*
x=0.0mol%	200	1.779E8	8.686E-10	1600	5.931E-6	0.39382	9.86E6	1.105E-8	0.962
x=0.5mol%	220	1.232E10	8.382E-10	500	2.645E-7	0.47536	6.844E8	3.631E-9	0.964
x=1.0mol%	306	1.732E11	6.461E-10	400	1.645E-9	0.76477	9.60E9	4.131E-9	0.964
x=1.5mol%	345	1.01E12	5.541E-10	380	1.164E-9	0.79783	5.61E10	6.535E-9	0.964